Structure and function of the archaeal response regulator CheY

Tessa E. F. Quax[a], Florian Altegoer[b], Fernando Rossi[a], Zhengqun Li[a], Marta Rodriguez-Franco[c], Florian Kraus[d], Gert Bange[b,1], and Sonja-Verena Albers[a,1]

[a]Molecular Biology of Archaea, Faculty of Biology, University of Freiburg, 79104 Freiburg, Germany; [b]Landes-Offensive zur Entwicklung Wissenschaftlich-ökonomischer Exzellenz Center for Synthetic Microbiology & Faculty of Chemistry, Philipps-University-Marburg, 35043 Marburg, Germany; [c]Cell Biology, Faculty of Biology, University of Freiburg, 79104 Freiburg, Germany; and [d]Faculty of Chemistry, Philipps-University-Marburg, 35043 Marburg, Germany

Edited by Norman R. Pace, University of Colorado at Boulder, Boulder, CO, and approved December 13, 2017 (received for review October 2, 2017)

Motility is a central feature of many microorganisms and provides an efficient strategy to respond to environmental changes. Bacteria and archaea have developed fundamentally different rotary motors enabling their motility, termed flagellum and archaellum, respectively. Bacterial motility along chemical gradients, called chemotaxis, critically relies on the response regulator CheY, which, when phosphorylated, inverses the rotational direction of the flagellum via a switch complex at the base of the motor. The structural difference between archaellum and flagellum and the presence of functional CheY in archaea raises the question of how the CheY protein changed to allow communication with the archaeal motility machinery. Here we show that archaeal CheY shares the overall structure and mechanism of magnesium-dependent phosphorylation with its bacterial counterpart. However, bacterial and archaeal CheY differ in the electrostatic potential of the helix α4. The helix α4 is important in bacteria for interaction with the flagellar switch complex, a structure that is absent in archaea. We demonstrated that phosphorylation-dependent activation, and conserved residues in the archaeal CheY helix α4, are important for interaction with the archaeal-specific adaptor protein CheF. This forms a bridge between the chemotaxis system and the archaeal motility machinery. Conclusively, archaeal CheY proteins conserved the central mechanistic features between bacteria and archaea, but differ in the helix α4 to allow binding to an archaellum-specific interaction partner.

chemotaxis | archaellum | CheY | motility | archaeal flagellum

The ability to respond to environmental changes and signals is of utmost relevance for all living organisms. One strategy is the directed movement toward and away from attractive and unfavorable signals, respectively (i.e., chemotaxis). To achieve this goal, microorganisms such as bacteria and archaea have developed sophisticated nanomachines that generate propulsive forces.

Archaea and bacteria use a rotating filamentous motility structure to swim: the archaellum and flagellum, respectively (1–4). Despite the functional similarities, the archaellum differs fundamentally from the well-studied bacterial flagellum (4, 5). It is constructed of proteins with homology to type IV pili, and its major subunits are made as preproteins (6–9). The rotary forces of the archaellum are generated by ATP hydrolysis instead of the proton motive force used to drive the flagellum in bacteria. New protein subunits of the archaellum are incorporated at the base of the growing filament, in contrast to the flagellum, in which subunits travel through the hollow interior to be added to the growing cap structure (10–12). Indeed, the recently published archaellum structure of *Methanospirillum hungatei* and *Pyrococcus furiosus* confirmed that the archaellum is not hollow and differs considerably from flagellum structures (13, 14). Not only are the filament of the archaellum and flagellum structurally different, but their motor complexes anchored in the membrane have completely divergent structures, as the proteins building them share no homology (15, 16).

Archaella and flagella can switch between clockwise and counterclockwise rotation (2, 17, 18). Several bacterial species display different swimming mechanisms. Counterclockwise rotation results in smooth swimming in well-characterized peritrichously flagellated bacteria such as *Escherichia coli*, whereas rotation in the opposite direction results in tumbling. In contrast, in other bacteria (i.e., *Vibrio alginolyticus*) and haloarchaea, clockwise rotation results in forward swimming, whereas counterclockwise rotation is responsible for swimming in the reverse direction (2, 18, 19). It is known that, in bacteria, the chemotaxis protein CheY plays a key role in directional switching of flagellar rotation, as it binds to the cytoplasmic switch complex of the flagellum to induce rotational switching of the flagellar motor in response to environmental signals sensed by chemosensory receptors (3, 20). The switch complex, or C-ring, of the flagellum is formed by the three proteins FliM, FliN, and FliG. This mechanism is well described and highly conserved among bacterial species (21). Briefly, stimulation of chemosensory receptors at the cytoplasmic membrane leads, via a signaling cascade, to the phosphorylation of CheY (CheY-P) (22, 23). First, CheY-P binds with high affinity to the N terminus of FliM. In a subsequent interaction, CheY binds to FliN that is in close association with the C-terminal domain of FliM (24, 25). Counterclockwise rotation of the flagellum involves the relative movement of FliN and the C-terminal domain of FliM (26, 27). The binding of CheY-P to FliM also causes the displacement of the C terminus of FliG that is interacting directly with components of the flagellar motor. Together, these alterations lead to a change in the

Significance

Motility is a key feature for the success of microorganisms, as it allows the movement to optimal growth environments. Bacteria and archaea possess filamentous motility structures capable of rotation. However, both molecular machines consist of fundamentally different proteins and lack structural similarity. Intriguingly, some archaea possess the chemotaxis system. This system allows bacteria to travel along chemical gradients and is dependent on interaction of the response regulator CheY with the motor of the motility structure. In this study, we map the changes of the CheY protein structure required for its interaction with components of the archaeal motility machinery.

Author contributions: T.E.F.Q., F.A., G.B., and S.-V.A. designed research; T.E.F.Q., F.A., F.R., Z.L., and M.R.-F. performed research; F.K. contributed new reagents/analytic tools; T.E.F.Q., F.A., M.R.-F., F.K., G.B., and S.-V.A. analyzed data; and T.E.F.Q., F.A., G.B., and S.-V.A. wrote the paper.

The authors declare no conflict of interest.

This article is a PNAS Direct Submission.

Data deposition: The atomic coordinates and structure factors have been deposited in the Protein Data Bank, www.pdb.org (PDB ID codes 6EKG and 6EKH).

[1]To whom correspondence may be addressed. Email: gert.bange@synmikro.uni-marburg.de or sonja.albers@biologie.uni-freiburg.de.

This article contains supporting information online at www.pnas.org/lookup/suppl/doi:10.1073/pnas.1716661115/-/DCSupplemental.

direction of swimming. A network of conserved amino acid residues enables an intricate allosteric communication between the phosphorylation and FliM binding sites of CheY (28). Phosphorylation of CheY requires a highly coordinated magnesium ion (29) and causes a coordinated rearrangement of the conserved tyrosine and threonine residues toward the active site (i.e., tyrosine 106 and threonine 87 in *E. coli* CheY, respectively) (30). These phosphorylation-induced molecular changes in CheY (also called Y-T coupling) remodel the FliM binding site of CheY and ensure that CheY-P binds with high affinity to FliM whereas CheY only binds with much lower affinity (28, 31–33). Many members of the archaea exhibit directed motility in response to various signals such as nutrients, oxygen, and light (34–39).

Interestingly, components of the chemotaxis system are present in Euryarchaea, Thaumarchaea, and the recently discovered deep-branching Lokiarchaea, and were likely acquired by horizontal gene transfer (40–43). The archaeal chemotaxis system belongs to the F1 class that is shared with bacteria from the *Firmicutes* and *Thermotogae*. It is hypothesized that the F1 class is the most ancestral system and was transferred from bacteria to euryarchaea (43). The model F1 chemotaxis system is that of *Bacillus subtilis*, which shares quite a few features with the archaeal chemotaxis systems (44). Study of the CheY protein of the archeon *Halobacterium salinarum* showed that, like in bacteria, CheY is phosphorylated and the protein and its phosphorylation state are essential for tactic behavior of archaea (45, 46). The flagellar proteins FliM and FliN that are the direct interaction partners of CheY-P in bacteria have no homologs in archaea (47). Instead, archaeal CheY is thought to interact with one or several adaptor proteins, named CheF, that were identified during a large protein–protein interaction study in *H. salinarum* (48, 49). CheF, in turn, in the same study, was reported to bind to FlaC, -D, and -E, which are euryarchaeal proteins with unknown function that are likely part of the archaellum motor complex (15, 48, 49). CheF belongs to the DUF439 archaeal protein family of unknown function (49). Its interaction with CheY was not characterized in detail. The structural difference between archaellum and flagellum and the presence of functional CheY in archaea raises the question of how the structure of the CheY protein was changed to allow communication with the archaeal motility machinery.

To determine whether the archaeal CheY indeed mediates chemosignaling and to map the structural changes required for communication with the archaeal motility machinery, we aimed to examine chemotactic performance in a euryarchaeal model. As there are only a limited number of archaeal species for which a genetic system is available and many archaea are thriving under extreme growth conditions (e.g., high salt, temperature), we first made a thorough analysis of available model systems. We opted for a dual approach of the euryarchaea *Haloferax volcanii* and *Methanococcus maripaludis*. For the halophile *H. volcanii*, one of the most advanced archaeal genetic systems is available, and it offers the distinct advantage of aerobic growth at moderate temperature (45 °C), allowing live imaging with thermomicroscopy. It contains a complete set of chemotaxis genes (CheB, C, D, R, W, Y, and archaeal-specific F), but its chemotactic behavior has not yet been studied. *H. volcanii* chemotaxis proteins display high homology with those of the anaerobic euryarchaeon *M. maripaludis*. Because of the suitability of *M. maripaludis* proteins (*Mm* proteins) for biochemical studies, we expressed and crystalized the euryarchaeal CheY from this system to characterize the structural determinants that may underlie the archaeal CheY function. This combinatory approach allowed us to conclude that archaeal CheY functions by a similar magnesium-dependent phosphorylation mechanism of activation as its bacterial counterpart. However, the archaeal CheY structure has, in contrast to bacterial CheY, a negatively charged region at the N terminus of the helix α4. Mutation of several residues in this region showed their importance for chemotaxis, as they affect the binding to the archaeal adaptor protein CheF, which links the chemotaxis system to the archaeal motility machinery. Our analysis highlights the structural changes that are needed to implement the original function of CheY as a response regulator into a fundamentally different motor structure.

Results

CheY-Mediated Directed Motility in the Archaeon *H. volcanii*. At first, we probed the putative role of CheY in regulating motility behavior in the genetically tractable euryarcheon *H. volcanii*. To achieve this aim, *cheY* was deleted in the WT strain H26 (Δ*pyrEF*) (50).

First we assessed if CheY influences biogenesis of archaella. Negative-stain EM of the Δ*cheY* strains revealed that the formation of archaella at the cell surface was not affected (*SI Appendix*, Fig. S1). As the ubiquitous adhesive pili of *H. volcanii* can hamper detection of the archaellum, this analysis was facilitated by also creating the *cheY* KO in the RE25 strain (Δ*pyrEF* Δ*pilB3-pilC3*; *Materials and Methods*), which lacks adhesive pili and therefore exclusively displays archaella at its surface (51). Δ*cheY* mutants in the RE25 background had the same phenotype as those in the H26 background (*SI Appendix*, Fig. S2). Cells of exponentially growing Δ*cheY* strains were still able to swim in liquid culture at 45 °C, demonstrating the presence of intact archaella (Movie S1). Together, these data show that CheY is not required for the biogenesis of the archaellum in *H. volcanii*.

However, closer inspection of the Δ*cheY* cells revealed that the number of swimming cells was lower than in WT. There seemed to be a tendency for smoother swimming behavior with a lower number of turns per second than the WT (*SI Appendix*, Fig. S3 and Movies S1 and S2). This observation is reminiscent of *cheY* deletions in the bacterium *E. coli* and the archeon *H. salinarum* that are well characterized to exhibit a "smooth swimming" phenotype (46, 52).

WT *E. coli* cells can move rapidly in search of nutrients on semisolid agar plates, forming visible motility rings. *E. coli* strains deficient in *cheY* are unable to perform this directed motility and therefore form smaller or no motility rings on semisolid agar plates. To assess whether our *H. volcanii* Δ*cheY* strain would also exhibit deficits in directional motility, exponentially growing cells were spotted on single semisolid agar plates made of rich medium and tryptophan (Fig. 1*A*). After 5 d of incubation, the diameters of the outer edge of the motility rings were measured, and the calculated relative diameters were compared with those formed by the WT strain. The Δ*cheY* strains did not form any motility rings on semisolid agar plates (Fig. 1). To confirm these observations, the Δ*cheY* strain was complemented with the empty pTA1228 plasmid and pTA1228 encoding WT CheY under a tryptophan-inducible promoter. Directional movement of the Δ*cheY* strain could be restored only when *cheY* was present (Fig. 1). Taken together, these data emphasize the role of CheY as a regulator of swimming behavior in response to nutrients in the model archaeon *H. volcanii*.

Characteristics of the Archaeal CheY Protein. To understand the changes in the CheY sequence required for communication with the archaellum, we studied similarities and differences of bacterial and archaeal CheY proteins by multiple sequence alignment (Fig. 2). This showed that several residues important for bacterial CheY function are conserved in archaea, such as the phosphorylation site (D51) and the aromatic residue reported in Y–T coupling (Y110) (32) (Fig. 2, blue arrows). Detailed experimental analysis of mutants of these residues was performed in bacteria. Mutation of the phosphorylation site of CheY in *E. coli* (D57) blocks directional movement of cells (53). It has been shown in *E. coli* that mutation of the aromatic residue involved in Y–T coupling (Y106) blocks directed movement (32). These mutants are unable to form motility rings on semisolid agar plates (53). We expected that these residues have a similar

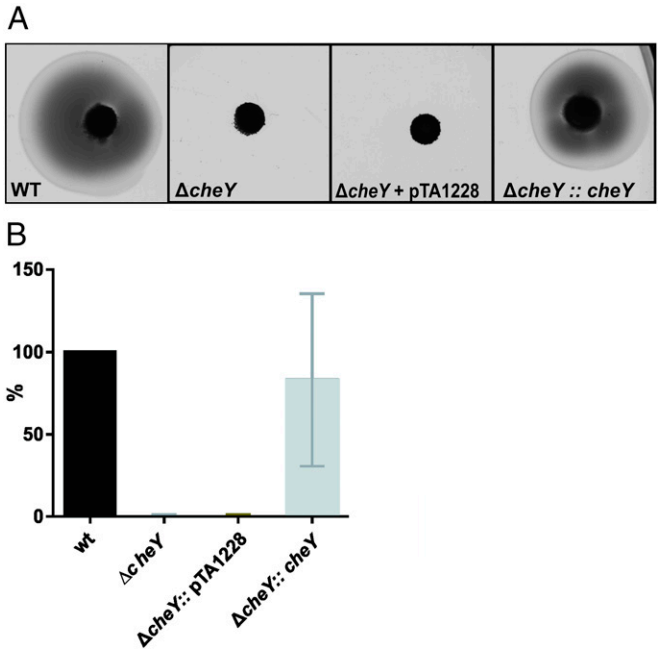

Fig. 1. Effect of CheY on directed movement in *H. volcanii*. Different plasmids were expressed in the *ΔcheY* background, strains spotted on semisolid agar plates made in rich medium, and plates scanned after 5 d. (*A*) Representative example of motility assay on semisolid agar plates of different *H. volcanii* strains. (*B*) Average diameter of motility rings, measured relative to the WT, from different *H. volcanii* strains from more than five independent experiments including four biological replicates each. pTA1228 is the empty plasmid. Error bar indicates SD. (Magnification: *A*, 0.7×.)

function in archaeal CheY and that, as a consequence, mutation of these residues will lead to a similar phenotype. In addition to the universally conserved residues, we selected amino acid residues conserved in euryarchaea and some bacteria with the F1 chemotaxis system (*Firmicutes* and *Thermotogae*). These residues are present mainly in a small region at the C terminus of CheY (i.e., Q95, E96). 95Q corresponds to K91 in *E. coli*, which is a reported acetylation site of CheY and confers clockwise rotation of the flagellum (54, 55). We hypothesized that these residues are important for archaeal CheY function and for connection to the archaellum, via interaction with its archaeal protein partner, CheF (49). Therefore, mutation of these sites might lead to reduced directional movement and altered swimming behavior.

Five alanine mutants were created and expressed from the same plasmid as native *cheY* to study their ability to restore directed movement the *ΔcheY* strain. First, exponentially growing cells of each strain were spotted together on semisolid agar plates containing varying concentrations of tryptophan for induction of expression. After 3–5 d of incubation at 45 °C, the motility rings were measured and compared with the WT and *ΔcheY* strain complemented with native *cheY*. Successful complementation with native *cheY* was observed on plates with different tryptophan levels. All five CheY amino acid mutations seemed to lead to reduced motility rings compared with the strain expressing native *cheY* (Fig. 3). The phosphorylation mutant *cheY_D51A* could not complement the WT, and no motility rings were formed at all. These observations suggest that phosphorylation of CheY is essential for its role in directing motility of archaea and agree with earlier biochemical experiments indirectly showing phosphorylation of CheY by CheA in the archaeon *H. salinarum* (37). The *cheY_Y110A*-expressing strain was generally not or only slightly capable of directed movement on semisolid agar plates, which corresponds with the reported phenotype of the similar amino acid substitution in *E. coli* (Y106). Taken together, these results indicate that the phosphorylation mechanism and Y–T coupling of CheY is conserved among bacteria and archaea.

In case of *cheY_E96A*, the diameter of motility rings was not strongly reduced. Interestingly, *cheY_C90A* and *cheY_Q95A* displayed a concentration-dependent phenotype as judged by the different size of their motility rings on semisolid agar plates made of rich medium with different concentrations of tryptophan. Whereas *cheY_C90A* cannot complement native *cheY* at low expression levels but can when the protein is highly expressed, the situation is reversed for *cheY_Q95A* (Fig. 3). On nutrient-limiting casamino acid (CA) plates, this concentration-dependent effect was not observed, and *cheY_95QA* did generally not form motility rings (*SI Appendix*, Fig. S4). The reduced diameter of motility rings of these five mutants indicates that the mutated residues are important for the function of archaeal CheY.

Effect of Amino Acid Substitutions of Archaeal CheY on Swimming Behavior. Next, we aimed to understand the cause of reduced directional movement in the five described CheY single amino acid mutants. Cells were grown under nutrient-limiting conditions. Cells of every strain were tracked, and their velocity in liquid medium was calculated in micrometers per second, in addition to the frequency of reversals, measured as the number of seconds between two subsequent turns (Fig. 4*A* and *B*). All *cheY* mutants showed, on average, similar swimming speeds of 3–5 μm/s, comparable to those of the WT and those reported previously (56). The exception was the *cheY_D51A*-expressing strain, of which the velocity could not be measured because almost no motile cells were observed. However, significant differences in the swimming behavior were observed for the other *cheY* mutants (Fig. 4*B* and *SI Appendix*, Table S2). *SI Appendix*, Fig. S5, displays the different frequency distribution of cells for each strain based on the number of seconds between two subsequent >90° turns. Two of the mutant *cheY* versions (i.e., *cheY_Q95A*, *cheY_E96A*) displayed an increased frequency of reversals compared with WT *cheY* (Fig. 4*B*, *SI Appendix*, Fig. S5, and Movies S3 and S4). Cells expressing *cheY_Q95A* were particularly switching direction so often that they covered only small distances (Fig. 4*B* and Movie S3). In contrast, expression of *cheY_Y110A* resulted in very smoothly swimming cells, which hardly changed direction at all (Movie S5). This is in accordance with the described phenotype of this aromatic residue variant in bacteria (32). In addition, expression of *cheY_C90A* also resulted in a smooth swimming phenotype, although the frequency of reversals was slightly higher than that of the *cheY_Y110A* mutant (Movie S6). The observed abnormal frequency of reversals of mutant cells expressing CheY versions with amino acid substitutions explains the reduced diameter of their motility rings on semisolid agar plates. Together, these experiments highlight the importance of these residues for CheY function.

Role of the Archaeal Adaptor Protein CheF. The mutational analysis of archaeal CheY described here indicates that it functions by a similar phosphorylation-dependent activation mechanism as its bacterial counterpart. In bacteria, phosphorylated CheY binds with higher affinity to the switch complex of the flagellar motor than in its inactive, nonphosphorylated form. Therefore, we analyzed whether phosphorylation of CheY could also be necessary for its interaction with the archaeal motility machinery. As already mentioned here earlier, a high-throughput interaction screening of chemotaxis proteins of *H. salinarum* suggested the interaction of CheY with the adaptor protein CheF, which is specific to archaea (49). Deletion of *cheF* showed that it is required for directed movement of *H. salinarum*. The screen also suggested that CheF interacts with structural proteins of the archaellum (i.e., FlaC, -D, and -E) (49). These observations

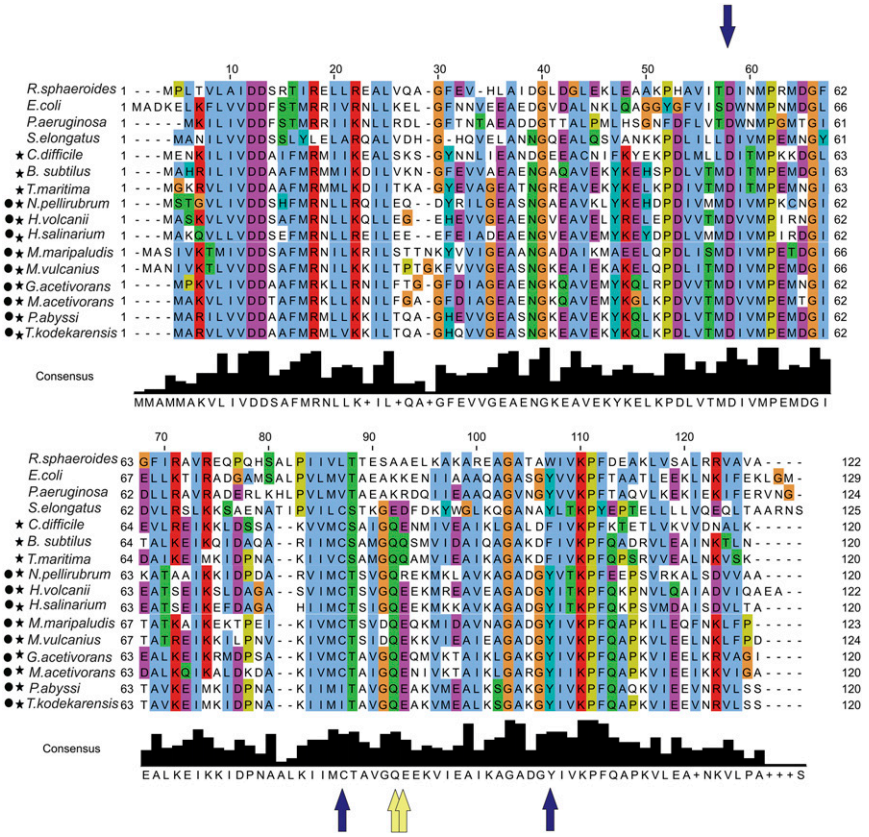

Fig. 2. Conserved and divergent amino acid residues between archaeal and bacterial CheY proteins. Multiple sequence alignment of the amino acid sequences of 20 representative CheY proteins from model euryarchaea and bacteria. Black dots in front of the species name indicate archaea. Stars indicate species with the F1-type chemotaxis system. Blue arrows indicate identical or similar amino acids conserved between bacteria and archaea that were selected for mutational analysis. Yellow arrows indicate identical or similar amino acids conserved in only archaea or in archaea plus *Firmicutes* and *Thermotogae*.

made CheF a promising interaction candidate for CheY, even though no detailed characterization of their interaction was available.

Therefore, we first assessed whether *cheF* would also be essential for the directed movement of *H. volcanii* on semisolid agar plates. Comparison of the size of motility rings with that of the WT showed that they were strongly reduced to <10% of the WT (Fig. 5 *A* and *B*). The WT phenotype could be restored by complementation with the native *cheF* gene. Observation by thermomicroscopy showed that cells of the *ΔcheF* strain were mainly smooth-swimming and the frequency of reversals was very low (Fig. 5*C*, *SI Appendix*, Fig. S8, and Movie S7). These results explain the reduced directional movement on semisolid agar plates and correspond with similar findings for the *ΔcheF* strain in *H. salinarum* (49). In addition to the main *cheF*, *H. volcanii* possess a second *cheF* copy in the archaellum-chemotaxis operon, named *cheF2* (28% identity with CheF). Although *cheF* is conserved in almost all chemotactic archaea, homologs of *cheF2* are found in only a very limited set of haloarchaea (49). A *ΔcheF2* strain was created and analyzed in the same way as the *ΔcheF1* strain. Deletion of *cheF2* resulted in only partially reduced motility rings on semisolid agar plates (35% of WT), and cells displayed approximately the same frequency of reversals as the WT (*SI Appendix*, Figs. S6 and S8 and Movie S8). These results indicate that *cheF2* probably has only a minor role in chemotaxis, which is in line with the described phenotype of the *cheF2* deletion in *H. salinarum* (49).

CheY–CheF Interaction. After establishing that CheF is important for chemotaxis in *H. volcanii*, we continued to characterize the possible interaction with CheY. As *H. volcanii* CheY (*Hv*CheY) and *Hv*CheF display strong homology with those of the euryarchaeon *M. maripaludis*, which are better suited for interaction studies, we purified *Mm*CheY (MMP0933) with a hexahistidine tag (his) and *Mm*CheF (MMP0934) with a Strep tag. In addition to CheY, *M. maripaludis* contains another gene annotated as response regulator (MMP1304), which is in contrast to CheY not located in the chemotaxis gene cluster and also displays less homology to *Hv*CheY and bacterial CheY sequences.

A pull-down assay was performed at 4 °C, and CheY-his served as bait on nickel-NTA mini columns. In the elution fraction, a faint band of the size of CheF could be observed on SDS/PAGE that could be confirmed as CheF by Western blotting with antibodies directed against the Strep tag present in CheF (Fig. 6 and *SI Appendix*, Fig. S9). To establish the importance of phosphorylation on the interaction, the same experiment was performed in the presence of beryllium fluoride (BeF_3^-). This compound has been widely used to mimic the phosphorylated state of bacterial CheY (57). In the presence of BeF_3^-, the interaction between CheY and CheF was significantly stronger in our Western blotting experiments (Fig. 6*A*). In addition to the beryllium fluoride, the assay was also performed with a CheY_D13K variant. In *E. coli*, this CheY variant cannot be dephosphorylated and is constantly in the active state (58). We verified that this is also the case in archaea and analyzed the phenotype of CheY_D13K mutant (*SI Appendix* and *SI Appendix*, Fig. S7). It was unable to form motility rings on semisolid agar plates, and analysis by microscopy showed that it has a very high frequency of reversals (*SI Appendix*, Figs. S7 and S8), as is the case for this mutation in *E. coli* CheY (59), but not for a

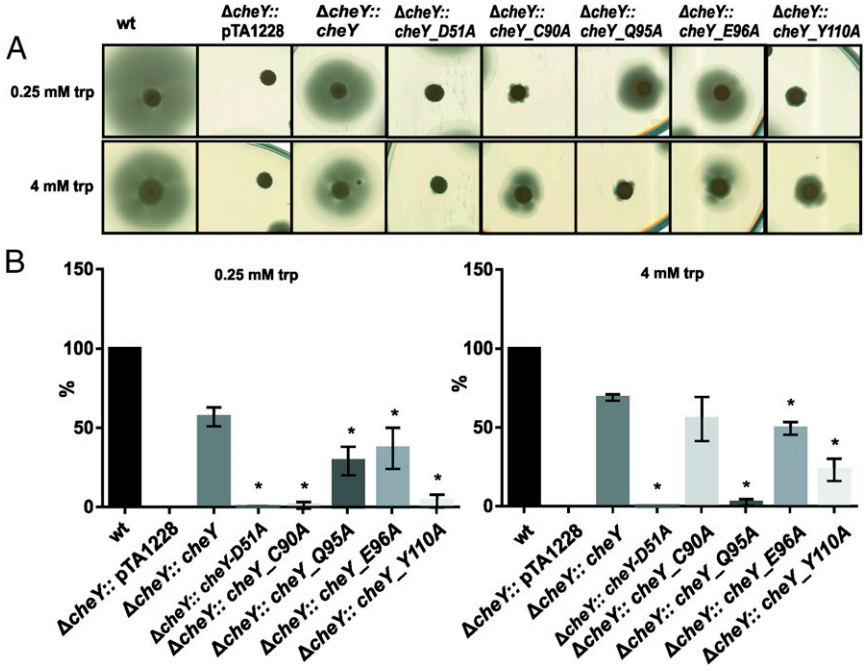

Fig. 3. Effect of conserved residues of the CheY protein on directional movement. Mutant versions of the *cheY* gene were expressed in a Δ*cheY* background of *H. volcanii*, strains spotted on semisolid agar plates made of rich medium, and plates scanned after 5 d. (*A*) Representative example of motility assays on semisolid agar plates of different *H. volcanii* strains after induction with varying concentrations of tryptophan. (*B*) Average diameter of motility rings, measured relative to the WT, from different *H. volcanii* strains from more than five independent experiments including four biological replicates each. The concentration of tryptophan is shown in the upper part of each graph. (*Left*) Low expression. (*Right*) High expression. Error bar indicates SD. pTA1228 is the empty plasmid. Asterisk indicates significantly different motility halos from strain expressing WT *cheY* ($P < 0.005$) as established by *t* test. (Magnification: *A*, 0.3×.)

similar mutation (D10K Y100W) in *H. salinarum* (60). Indeed, the pull-down analysis at 4 °C showed that the archaeal CheY_D13K binds with higher affinity to CheF compared with WT in absence of BeF_3^- (Fig. 6*A*). The same pull-down experiment was also performed at 37 °C. In this case, the interaction with CheF was similar for the WT CheY, the WT CheY in the presence of BeF_3^- and the CheY_D13K mutant (Fig. 6*A*). Taken together, these results demonstrate that the chemotaxis system requires a specific adaptor protein, CheF, for interaction with the archaellum motility machinery, and that this interaction is stronger when CheY is in activated state after phosphorylation. This resembles the binding mechanism of bacterial CheY to FliM of the switch complex of the flagellum.

In addition, we also studied the CheY–CheF interaction by using CheY amino acid substitution mutants that affect swimming behavior in *H. volcanii*. In a similar experimental setup as described here earlier, a pull-down was performed between *Mm*CheF and mutant versions of CheY (CheY_C90A, CheY_Q95A, CheY_E96A). Analysis of the elution fractions by SDS/PAGE, Western blotting, and immune detection with anti-Strep antibody showed that the interaction of CheF with CheY_Q95A was comparable with WT CheY (Fig. 6*B* and *SI Appendix*, Fig. S9). However, in comparison with WT CheY, the intensity of the CheF band was much reduced after a pull-down with CheY_C90A (Fig. 6*B* and *SI Appendix*, Fig. S9). Mutation of this site has a negative effect on the affinity of CheY for CheF. In contrast, the CheY_E96A mutant bound more strongly to CheF compared with WT CheY (Fig. 6*B* and *SI Appendix*, Fig. S9). These findings indicate that the altered frequency of reversals of CheY amino acid substitutions mutants is caused by their altered interaction with the CheF adaptor protein.

Phosphorylation Mechanism Is Conserved Among Archaeal CheYs. Finally, to characterize the structural determinants that may underlie the archaeal CheY function, we aimed to resolve its mechanism at atomic resolution. Because of the high ionic strength required for correct folding of *H. volcanii* proteins, we purified the highly homologous CheY protein (MMP0933) from the related euryarcheon *M. maripaludis*. Well-diffracting crystals of *Mm*CheY protein could be obtained. To investigate whether the activation mechanism is also conserved among archaeal CheYs, we also crystallized *Mm*CheY in the presence of 2 mM BeF_3^- and 20 mM NaF as described previously for the bacterial homolog (61).

A central feature of bacterial CheY proteins is their phosphorylation at a conserved aspartate accompanied by the coordination of a magnesium ion. We therefore wanted to elucidate the phosphorylation mechanism of archaeal CheY to understand whether it is fundamentally different from the bacterial one (Fig. 7*A*). Thus, we superimposed the apo- and BeF_3^--bound state and investigated structural differences between the two states. The models superimposed well with an rmsd over all Cα atoms of 0.465 $Å^2$. Upon activation by BeF_3 binding, the β4–α4 loop and adjacent regions are displaced as previously described for bacterial CheYs (Fig. 7*A*, *Right*) (61, 62). A closer inspection of important residues, namely D57, which becomes phosphorylated (D51 in *H. volcanii*), T85 and Y104 (Y110 in *H. volcanii*) showed that the threonine and tyrosine residues are displaced upon activation, whereas D57 stays in position (Fig. 7*B*). Furthermore, the amino acid residues D12 and D57 and the backbone oxygen of V59 coordinate the magnesium ion together with three water molecules (*SI Appendix*, Fig. S10*A*). Structural comparison of the *Mm*CheY with other bacterial CheY homologs shows that this magnesium ion-binding site, as well as the phosphate group receiving aspartate (D57 in *Mm*CheY), is structurally conserved (*SI Appendix*, Fig. S10*B*). We compared the structure of activated *Mm*CheY with a structure of an activated CheY of *E. coli* [Protein Data Bank (PDB) ID code 1FQW] to find out whether phosphorylation had the same effect on structural rearrangements in bacteria and archaea. Both structures align very well with an rmsd over all Cα atoms of

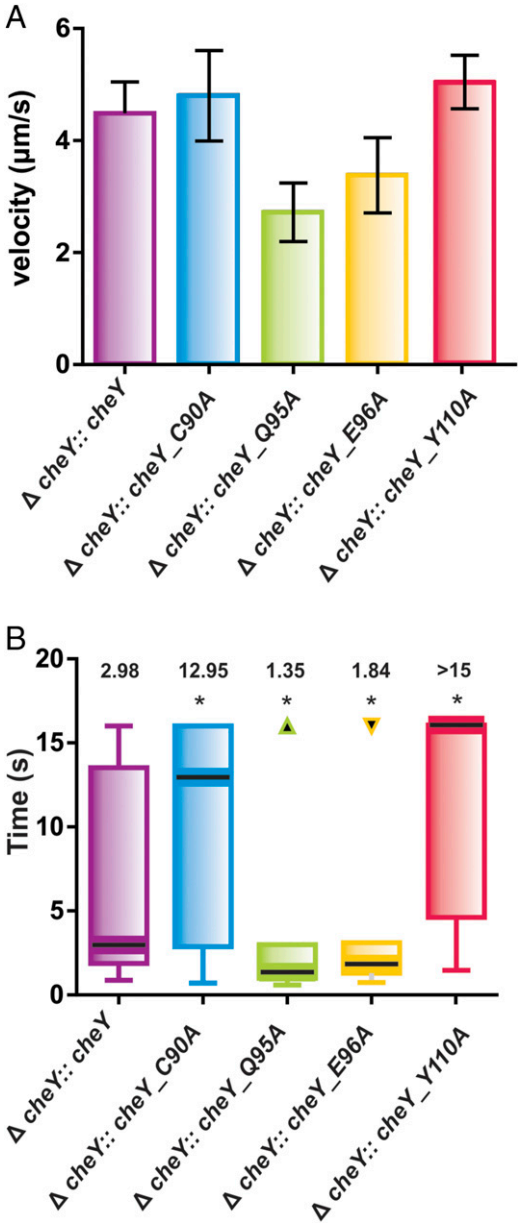

Fig. 4. Effect of conserved residues of the CheY protein on swimming behavior. Mutant versions of the *cheY* gene were expressed in a Δ*cheY* background of *H. volcanii*, and liquid cultures were analyzed by light microscopy at 45 °C. (*A*) Average velocity of different strains. Bars indicate SD. (*B*) Tukey box plot of number of seconds between two subsequent turns of >90°. For each strain, the median is displayed above the respective bar and indicated by a black horizontal line. Boxes display the 25–75th percentile, and bars represent the minimum and maximum time. Triangles indicate maximum outliers. Asterisk indicates significantly different swimming behavior from strain expressing WT *cheY* ($P < 0.0001$) as established by Wilcoxon–Mann–Whitney test (*SI Appendix*, Table S2).

0.97 Å. Conserved residues (D57, T85/87, Y104/106) can be almost perfectly superimposed (Fig. 7*C*). These structural rearrangements are also conserved in the F1-type CheY from *T. maritima* (PDB ID code 4IGA; rmsd over all Cα atoms, 0.683 Å), although some of the respective residues have been replaced (i.e., T85 to S82 and Y104 to F101; Fig.7*D*).

Taken together, our structural and functional assays show that the phosphorylation mechanism is conserved among archaea and bacteria.

Archaeal-Specific Changes in the CheY Structure. In bacteria, CheY-P binds to the N terminus of the C-ring protein FliM (FliM-N), including the conserved "EIDAL" motif (33, 62, 63). Earlier crystallographic analysis showed that an extended surface groove formed by helices α4 and α5 and the strand β5 of CheY serves as interaction site of FliM-N. Although FliM-N can bind with low affinity to CheY, its interaction with CheY-P is significantly higher as a result of a phosphorylation-dependent reorientation of Y106 located within β5 (28). Furthermore, rearrangement of the β4–α4 loop upon phosphorylation can be observed in *Mm*CheY, similar to the displacement in *E. coli* (Fig. 7*C*). A second binding site for FliM-N at CheY has been reported in *T. maritima* involving Met14 and Gln107 (64). These residues are conserved in archaeal CheY and might therefore also be involved in CheF binding.

Moreover, the bacterial CheY/FliM-N interface is stabilized by a combination of hydrophobic interactions, hydrogen bonds, and salt bridges. Comparison of the FliM interaction sites shows slight differences between bacterial and archaeal CheY proteins. Although the region corresponding to the FliM-N binding site of bacterial CheY is mostly conserved on sequence and structural levels in archaea and bacteria (Fig. 2), a specific residue in the N-terminal part of α4 exhibits a different electrostatic potential (Fig. 8). In *Mm*CheY, a glutamate occupies this position (Fig. 8*A*), which is replaced by a glutamine in *Tm*CheY (Fig. 8*B*) and a lysine in *Ec*CheY (Fig. 8*C*).

This observation suggests that archaeal CheY proteins have a slightly different interaction surface, which allows binding to

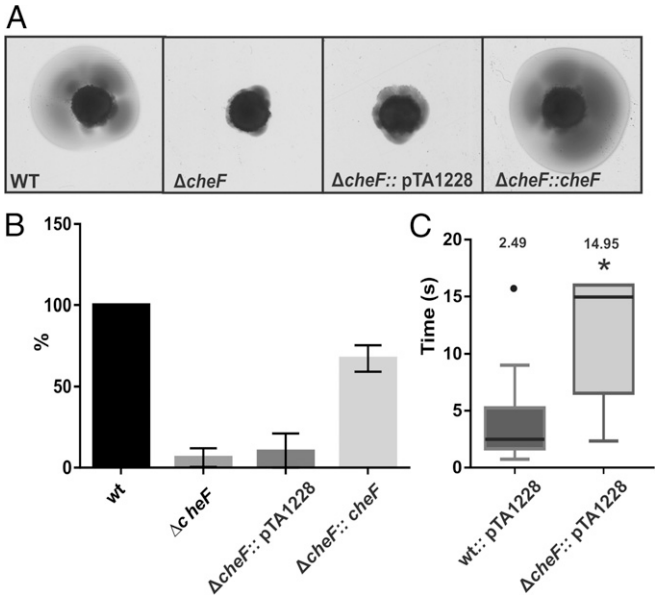

Fig. 5. Role of archaeal adaptor protein CheF. Effect of CheF on directed movement in *H. volcanii H26* in rich medium. Different plasmids were expressed in the Δ*cheF* background, strains spotted on semisolid agar plates, and plates scanned after 5 d. (*A*) Representative example of motility assay on semisolid agar plates of different *H. volcanii* strains. (*B*) Average diameter of motility rings, measured relative to the WT, from different *H. volcanii* strains from more than three independent experiments including three biological replicates each. pTA1228 is the empty plasmid. Error bar indicates SD. (*C*) Analysis of swimming behavior of different *H. volcanii* mutants as observed with time-lapse movies on the thermomicroscope. Tukey box plot of number of seconds between two subsequent turns of >90° of a cell. For each strain, the median is displayed above the respective bar and indicated by a black horizontal line. Boxes display the 25–75th percentile and bars represent the minimum and maximum time. Circle indicates maximum outliers. Asterisk indicates significantly different swimming behavior from WT ($P < 0.005$) as established by *t* test (*SI Appendix*, Table S2). (Magnification: *A*, 0.7×.)

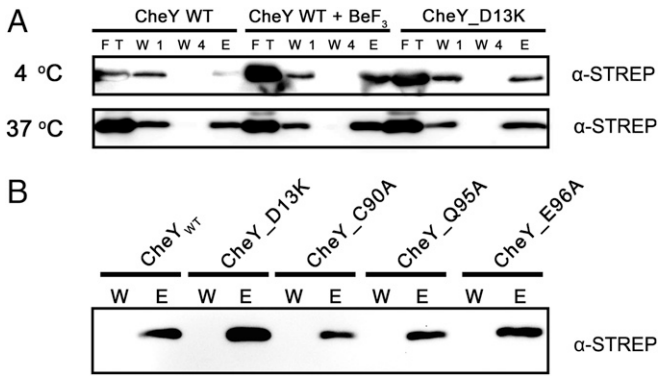

Fig. 6. Interaction of CheY and CheF. (*A*) Representative Immunoblot with α-strep antibody on pull-down to detect CheF of *M. maripaludis* using CheY-his as bait and CheF-Strep as prey in the presence or absence BeF_3^- (*B*) Immunoblot with α-Strep antibody on pull-down to detect CheF of *M. maripaludis* using mutant versions of CheY-his as bait and CheF-Strep as prey. Experiment was performed at 37 °C. Both experiments were performed more than times. E, elution; FT, flow-through; W1, first wash; W4 or W, last wash. Representative SDS gels of this experiment are shown in *SI Appendix*, Fig. S9.

the archaeal CheF protein. Although most residues that contribute to bacterial FliM-N binding seem to be conserved among bacteria and archaea, the negative charge present at the N-terminal end of helix a4 seems to be a specialty of archaea. This idea agrees with the observations that the archaellum lacks a C-ring and archaeal genomes do not encode for FliM proteins or any other flagellum components.

Discussion

Archaea and bacteria possess fundamentally different motility structures: archaella and flagella, respectively. However, some archaea possess the chemotaxis system, including the important response regulator protein CheY, which they likely received from bacteria via horizontal gene transfer (43, 41). Whereas CheY interacts with the base of the flagellum in bacteria to achieve directed movement, archaeal CheY should interact with the base of the archaellum.

Important residues of the CheY protein, such as the phosphorylation site and those involved in Y–T coupling, are conserved between bacteria and archaea. Replacement of the aspartate at position 57 by an alanine in archaeal CheY led to cells incapable of directed movement, as is the case for a similar mutation in the bacterial CheY (55). In addition, the aromatic residue important for Y–T coupling (Y110 in *H. volcanii*) is conserved between bacteria and archaea. Replacement of this residue by a nonaromatic amino acid led to reduced directional movement on motility plates and a smooth swimming behavior in *H. volcanii*. A similar phenotype has been observed in bacteria, in which it was shown that this mutation does not influence the binding efficiency of CheY to FliM (32). The *cheY_C90A* substitution results in an inactive CheY. Indeed, the binding of CheY to the archaeal-specific CheF protein was reduced when *C90* was mutated. Cells carrying this variant swim smoothly and have a low frequency of reversals. This phenotype resembles the phenotype of the *cheY_Y110A* mutant. It is possible that mutation of C90 influences the neighboring T91 (T87 in *E. coli*) that is involved in T–Y coupling. Our observations show that, in archaea, this aromatic residue is also important for the signal transduction of CheY. By resolving the crystal structure of archaeal CheY, we show that the residues important for activation upon phosphorylation rearrange in a similar way as the bacterial CheY.

Our study of the archaeal CheY shows that CheY structure and activation mechanism are conserved between archaea and bacteria. However, archaeal CheY should interact with the archaellum motor complex instead of the bacterial FliM protein. Previously, an interactome study in the archeon *H. salinarum* suggested that the adaptor protein CheF mediates the interaction between CheY and components of the archaellum (i.e., FlaC, -D, and -E) (48, 49). We now confirm that CheF is indeed required for

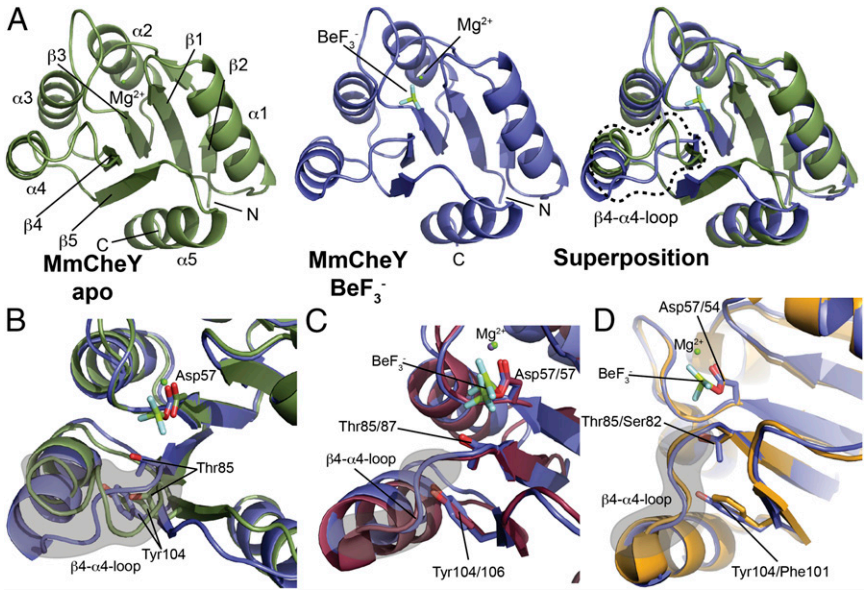

Fig. 7. Mechanism of CheY activation is conserved among archaea and bacteria. (*A*) Comparison of apo- and BeF_3-activated CheY in *M. maripaludis*. CheY of *M. maripaludis* resembles the overall fold observed for CheY homologs from different bacterial species (green). Upon activation by BeF_3, the α4–β4 loop rearranges, as well as α4 and β5 (blue). (*B*) Close-up of rearrangements upon activation. Apo-CheY is shown in smudge green and CheY-BeF_3 in blue. (*C*) Activated CheY from *E. coli* and *M. maripaludis* show the same rearrangements. *Ec*CheY (PDB ID code 1FQW) and *Mm*CheY can be superimposed well, and positions of conserved Asp, Thr, and Tyr residues show almost no displacement. (*D*) Activated CheY from *T. maritima* and *M. maripaludis* show the same rearrangements. *Tm*CheY (PDB ID code 4IGA) and *Mm*CheY can be superimposed well, and positions of the slightly varied Asp, Thr(Ser), and Tyr(Phe) residues show almost no displacement. Residues in brackets represent the *T. maritima* residues.

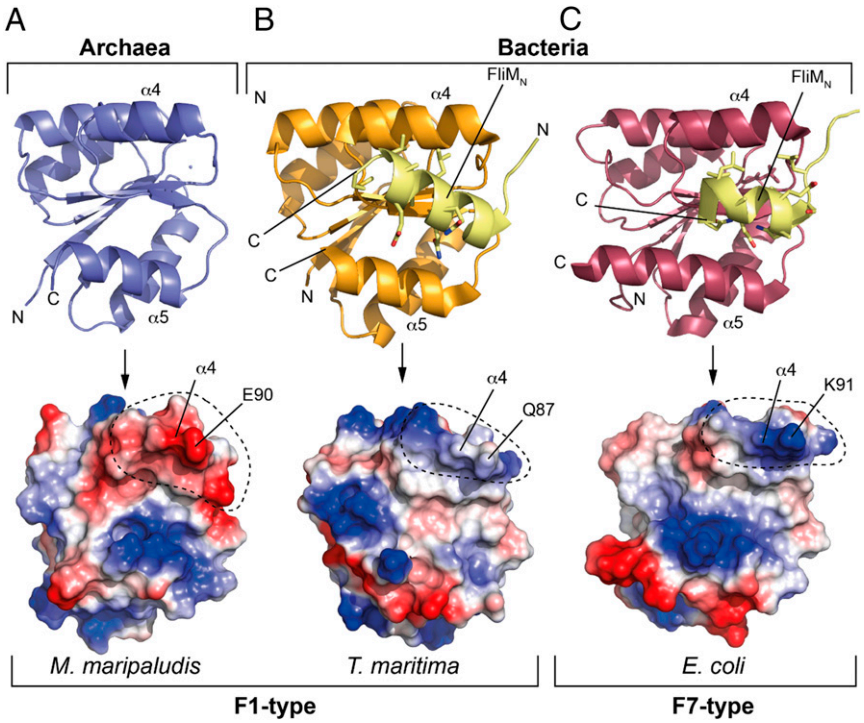

Fig. 8. The CheY from *M. maripaludis* shows archaeal-specific adaptations. Comparison of (*A*) *Mm*CheY, (*B*) TmCheY-FliM$_{16}$ (PDB ID code 4IGA), and (*C*) EcCheY-FliM$_{16}$ (PDB ID code 1F4V). (*Upper*) Models are shown in cartoon representation. Side chains of FliM$_N$ are depicted as sticks and colored according to their elements. (*Lower*) Surface electrostatic representation shows a prominent negative charge within the N-terminal region of α4 in the archaeal CheY that is absent in the bacterial CheY. Furthermore, the CheY homologs from the F-1 type form rather compact particles and have a shorter α5 helix.

directional movement and show that the *ΔcheF* strain displays reduced directional movement, as these mutants have a very low frequency of reversals. In addition, we demonstrate that the CheY–CheF interaction is phosphorylation-dependent in a similar fashion as the CheY–FliM interaction in bacteria. WT archaeal CheY can bind CheF with low affinity. Binding is increased significantly when the phosphorylated state is mimicked by adding BeF_3^- as has been used in several studies with bacterial CheY (57, 61). Similarly, the interaction with CheF is enhanced when CheY_D13K mutant, locked in active state, is used in binding assays. These results indicate that the phosphorylation-dependent activation mechanism of archaeal and bacterial CheY is conserved. Indeed, resolution of the archaeal CheY structure showed that its overall fold is very similar to bacterial CheY structures. Binding to the archaeal adaptor protein CheF might occur in a similar fashion as binding to bacterial FliM.

Besides the similarities, there are also clearly definable differences between archaeal and bacterial CheY. Detailed comparison of the archaeal and bacterial protein shows that a residue at the N-terminal end of helix α4 of CheY is positively charged (in *E. coli*) or uncharged (in *T. maritima*), whereas this residue in archaea exhibits a prominent negative charge. Two conserved residues in the N terminus of the helix α4 (i.e., Q95 and E96) were substituted, and analysis of the directional movement and swimming behavior in mutant cells showed that this leads to significantly different swimming behavior vs. WT CheY. The *cheY_Q95A* and *cheY_E96A* mutations lead to cells with a very high frequency of reversals. In this they resemble bacterial strains with mutations in *cheZ* or *cheB*, which lead to a tumbling phenotype, as CheY is not efficiently dephosphorylated (53, 65). In *E. coli*, several amino acid substitutions in CheY can also lead to phenotypes with frequent reversals and tumbling. In case of a Y106W substitution, frequent reversals occur, and the activity of this *cheY* mutant is phosphorylation-dependent (32). The D13K substitution results in tumbling cells as a result of a constantly active CheY (58, 66). Also, the T87A (67), F14R (68), N23D (69), N59R (70), I95V (71), and N94T (72) mutations in CheY are reported to result in more frequent reversals, although the exact mechanism remains unclear. Interestingly, in *E. coli*, acetylation of the lysine residue at position 92 (corresponding to Q95 in *H. volcanii* CheY) was reported to convert clockwise rotation of the flagellum, resulting in cell tumbling (55, 73). Acetylation reduces affinity of CheY for FliM (74). Mutation of this site in *E. coli* represses clockwise rotation (54). Acetylation of this position is important for switching between active and inactive states of CheY in *E. coli* (54). The bacterium *T. maritima* has the type F1 chemotaxis system and shares the glutamine on similar position (Q86). It has been hypothesized that this glutamine in *T. maritima* plays a role in enhancement of the stability of the β4–α4 loop in its inactive conformation and that it inhibits the conformational shift to the active form. This hypothesis corresponds well with the finding that expression of *cheY_Q95A* and *cheY_E96A* leads to CheY locked in the active state, resulting in cells with a high frequency of reversals. In addition, the mutant expressing *cheY_E96A* also displays significantly enhanced binding affinity to the archaeal-specific adaptor protein CheF, indicating an active state.

In archaea, this region is important for interaction with the motility machinery, and the charge differences may represent changes required for interaction with the archaeal-specific partner protein CheF. Future cocrystallization studies might reveal how archaeal CheY is able to bind with the archaeal specific CheF while maintaining the ability to bind to conventional chemotaxis proteins (i.e., CheA).

Taken together, the results described here demonstrate that archaeal CheY acts by a similar mechanism as its bacterial counterparts. However, changes in helix α4 of CheY allow the archaeal CheY to interact with archaeal-specific partners of the

chemotaxis and motility system. As such, the chemotaxis system requires certain structural changes in its response regulator to efficiently communicate with the different motility structures in bacteria and archaea.

Materials and Methods

Growth and Genetic Manipulation *H. volcanii*. *H. volcanii* strains were grown as described previously (50). Genetic manipulation based on selection with uracil in Δ*pyrE2* strains was carried out with PEG 600 as described previously (50). To create KO strains, plasmids based on pTA131 were used carrying a *pyrE2* cassette in addition to ∼500-bp flanking regions of the targeted gene (50). For expression of proteins, plasmids based on pTA1228 (75) were constructed, carrying the pyrE2 cassette and a gene under control of the tryptophan promoter.

Strains, Plasmids, and Primers. Strains, plasmids, and primer sequences used in this study are detailed in *SI Appendix*, Tables S3–S5.

Motility Assay for *H. volcanii* on Semisolid Agar Plates. The motility assay experiment was performed mainly as described by Tripepi et al. (76) based on assays in *E. coli* by Adler et al. (77). Fresh cells from agar plates were used to inoculate 5-mL precultures grown in CA medium, complemented with 50 μg/mL uracil and/or tryptophan when required. Large semisolid agar plates of 0.3% agar were freshly prepared with yeast peptone casamino acid or CA medium containing 0.25 or 4 mM tryptophan. The plates were inoculated with drops of 10 μL of culture of each strain and incubated for 4–5 d.

EM. *H. volcanii* RE25 (51) and HTQ17 cells were grown over night in CA medium to OD 0.2 and fixed with 2% (vol/vol) glutaraldehyde and 1% (vol/vol) formaldehyde in CA medium, negatively stained with 2% (wt/vol) uranyl acetate, and imaged by using a CM10 transmission electron microscope (Philips) coupled to a Gatan 792 BioScan camera.

Light Microscopy Swimming Behavior. One milliliter of culture was placed in a round DF 0.17-mm microscopy dish (Bioptechs) and observed at 63× magnification in the DICII mode with an Axio Observer 2.1 microscope (Zeiss) equipped with a heated XL-5 2000 Incubator running VisiVIEW software. Cells in recorded 15-s time-lapse movies were tracked later by using Metamorph software and *x*,*y* coordinates were calculated. From the *x*,*y* coordinates, the average velocity and the number of turns larger than 90° of a given time frame was calculated for each cell by using the Pythagoras theorem.

Protein Purification. CheY protein production and purification was performed as described earlier (78). CheF protein purification was performed as described in *SI Appendix, SI Materials and Methods*.

Crystallization. All crystallization experiments were carried out by the sitting-drop method in SWISSCI-MRC two-well crystallization plates at room temperature. Crystals of *M. maripaludis* CheY were obtained from a 20.0-mg/mL solution after 24 h in 0.2 M magnesium formate, 20% PEG 3350. The crystallization of activated *Mm*CheY was performed at a concentration of 20.0 mg/L in the presence of 2 mM BeF and 20 mM NaF. Crystals were obtained after 24 h in 0.2 M NaCl, 0.1 M Hepes, pH 7.5, and 20% PEG 3000. Data collection was performed at beamline ID30A-1 (MASSIF-1; ref. 79) under cryogenic conditions at the European Synchrotron Radiation Facility in Grenoble, France.

Data Collection, Structure Determination, and Analysis. Data were integrated and scaled with XDS (80) and merged with ccp4-implemented AIMLESS (81). Structures were determined by molecular replacement with PHASER (82), manually built in COOT (83), and refined with PHENIX (84). Detailed descriptions of study materials and methods are provided in the *SI Appendix*.

ACKNOWLEDGMENTS. We thank the European Synchrotron Radiation Facility for support and Marleen van Wolferen for advice on thermomicroscopy. This study was supported by a Marie-Curie Intra-European Fellowship (to T.E.F.Q.), Collaborative Research Center Grant 746 from the Deutsche Forschungsgemeinschaft (to S.-V.A.), European Research Council Starting Grant ARCHAELLUM 311523 (to F.R.), the China Scholarship Council (Z.L.), and the Landes-Offensive zur Entwicklung Wissenschaftlich-ökonomischer Exzellenz program of the state of Hesse (G.B.).

1. Berg HC, Anderson RA (1973) Bacteria swim by rotating their flagellar filaments. *Nature* 245:380–382.
2. Alam M, Oesterhelt D (1984) Morphology, function and isolation of halobacterial flagella. *J Mol Biol* 176:459–475.
3. Chevance FF, Hughes KT (2008) Coordinating assembly of a bacterial macromolecular machine. *Nat Rev Microbiol* 6:455–465.
4. Jarrell KF, Albers SV (2012) The archaellum: An old motility structure with a new name. *Trends Microbiol* 20:307–312.
5. Altegoer F, Bange G (2015) Undiscovered regions on the molecular landscape of flagellar assembly. *Curr Opin Microbiol* 28:98–105.
6. Kalmokoff ML, Jarrell KF (1991) Cloning and sequencing of a multigene family encoding the flagellins of Methanococcus voltae. *J Bacteriol* 173:7113–7125.
7. Bardy SL, Jarrell KF (2003) Cleavage of preflagellins by an aspartic acid signal peptidase is essential for flagellation in the archaeon Methanococcus voltae. *Mol Microbiol* 50:1339–1347.
8. Szabó Z, Albers SV, Driessen AJ (2006) Active-site residues in the type IV prepilin peptidase homologue PibD from the archaeon Sulfolobus solfataricus. *J Bacteriol* 188:1437–1443.
9. Szabó Z, et al. (2007) Identification of diverse archaeal proteins with class III signal peptides cleaved by distinct archaeal prepilin peptidases. *J Bacteriol* 189:772–778.
10. Jarrell KF, Bayley DP, Kostyukova AS (1996) The archaeal flagellum: A unique motility structure. *J Bacteriol* 178:5057–5064.
11. Cohen-Krausz S, Trachtenberg S (2008) The flagellar filament structure of the extreme acidothermophile Sulfolobus shibatae B12 suggests that archaeabacterial flagella have a unique and common symmetry and design. *J Mol Biol* 375:1113–1124.
12. Cohen-Krausz S, Trachtenberg S (2002) The structure of the archeabacterial flagellar filament of the extreme halophile Halobacterium salinarum R1M1 and its relation to eubacterial flagellar filaments and type IV pili. *J Mol Biol* 321:383–395.
13. Poweleit N, et al. (2016) CryoEM structure of the Methanospirillum hungatei archaellum reveals structural features distinct from the bacterial flagellum and type IV pili. *Nat Microbiol* 2:16222.
14. Daum B, et al. (2017) Structure and *in situ* organisation of the *Pyrococcus furiosus* archaellum machinery. *Elife* 6:e27470.
15. Chaban B, et al. (2007) Systematic deletion analyses of the fla genes in the flagella operon identify several genes essential for proper assembly and function of flagella in the archaeon, Methanococcus maripaludis. *Mol Microbiol* 66:596–609.
16. Lassak K, et al. (2012) Molecular analysis of the crenarchaeal flagellum. *Mol Microbiol* 83:110–124.
17. Berg HC, Brown DA (1972) Chemotaxis in Escherichia coli analysed by three-dimensional tracking. *Nature* 239:500–504.
18. Shahapure R, Driessen RP, Haurat MF, Albers SV, Dame RT (2014) The archaellum: A rotating type IV pilus. *Mol Microbiol* 91:716–723.
19. Xie L, Altindal T, Chattopadhyay S, Wu X-L (2011) From the cover: Bacterial flagellum as a propeller and as a rudder for efficient chemotaxis. *Proc Natl Acad Sci USA* 108:2246–2251.
20. Sourjik V, Berg HC (2002) Binding of the Escherichia coli response regulator CheY to its target measured in vivo by fluorescence resonance energy transfer. *Proc Natl Acad Sci USA* 99:12669–12674.
21. Porter SL, Wadhams GH, Armitage JP (2011) Signal processing in complex chemotaxis pathways. *Nat Rev Microbiol* 9:153–165.
22. Welch M, Oosawa K, Aizawa S, Eisenbach M (1993) Phosphorylation-dependent binding of a signal molecule to the flagellar switch of bacteria. *Proc Natl Acad Sci USA* 90:8787–8791.
23. Parkinson JS, Hazelbauer GL, Falke JJ (2015) Signaling and sensory adaptation in Escherichia coli chemoreceptors: 2015 update. *Trends Microbiol* 23:257–266.
24. Barak R, Eisenbach M (1992) Correlation between phosphorylation of the chemotaxis protein CheY and its activity at the flagellar motor. *Biochemistry* 31:1821–1826.
25. Porter SL, et al. (2006) The CheYs of Rhodobacter sphaeroides. *J Biol Chem* 281:32694–32704.
26. Sarkar MK, Paul K, Blair D (2010) Chemotaxis signaling protein CheY binds to the rotor protein FliN to control the direction of flagellar rotation in Escherichia coli. *Proc Natl Acad Sci USA* 107:9370–9375.
27. Paul K, Brunstetter D, Titen S, Blair DF (2011) A molecular mechanism of direction switching in the flagellar motor of Escherichia coli. *Proc Natl Acad Sci USA* 108:17171–17176.
28. Dyer CM, Dahlquist FW (2006) Switched or not?: The structure of unphosphorylated CheY bound to the N terminus of FliM. *J Bacteriol* 188:7354–7363.
29. Stock AM, et al. (1993) Structure of the Mg(2+)-bound form of CheY and mechanism of phosphoryl transfer in bacterial chemotaxis. *Biochemistry* 32:13375–13380.
30. Bellsolell L, Prieto J, Serrano L, Coll M (1994) Magnesium binding to the bacterial chemotaxis protein CheY results in large conformational changes involving its functional surface. *J Mol Biol* 238:489–495.
31. Ganguli S, Wang H, Matsumura P, Volz K (1995) Uncoupled phosphorylation and activation in bacterial chemotaxis. The 2.1-A structure of a threonine to isoleucine mutant at position 87 of CheY. *J Biol Chem* 270:17386–17393.
32. Zhu X, Amsler CD, Volz K, Matsumura P (1996) Tyrosine 106 of CheY plays an important role in chemotaxis signal transduction in Escherichia coli. *J Bacteriol* 178:4208–4215.
33. Lee SY, et al. (2001) Crystal structure of an activated response regulator bound to its target. *Nat Struct Biol* 8:52–56.
34. Spudich Walther JLS (1979) Photosensory and chemosensory behavior of Halobacterium halobium. *Photobiochem Photobiophys* 1:43–53.
35. Marwan W, Oesterhelt D (1987) Signal formation in the halobacterial photophobic response mediated by a fourth retinal protein (P480). *J Mol Biol* 195:333–342.

36. Lindbeck JC, Goulbourne EA, Jr, Johnson MS, Taylor BL (1995) Aerotaxis in Halobacterium salinarium is methylation-dependent. *Microbiology* 141:2945–2953.
37. Rudolph J, Oesterhelt D (1995) Chemotaxis and phototaxis require a CheA histidine kinase in the archaeon Halobacterium salinarium. *EMBO J* 14:667–673.
38. Storch KF, Rudolph J, Oesterhelt D (1999) Car: A cytoplasmic sensor responsible for arginine chemotaxis in the archaeon Halobacterium salinarum. *EMBO J* 18: 1146–1158.
39. Kokoeva MV, Oesterhelt D (2000) BasT, a membrane-bound transducer protein for amino acid detection in Halobacterium salinarum. *Mol Microbiol* 35:647–656.
40. Wuichet K, Cantwell BJ, Zhulin IB (2010) Evolution and phyletic distribution of two-component signal transduction systems. *Curr Opin Microbiol* 13:219–225.
41. Briegel A, et al. (2015) Structural conservation of chemotaxis machinery across Archaea and Bacteria. *Environ Microbiol Rep* 7:414–419.
42. Spang A, et al. (2015) Complex archaea that bridge the gap between prokaryotes and eukaryotes. *Nature* 521:173–179.
43. Wuichet K, Zhulin IB (2010) Origins and diversification of a complex signal transduction system in prokaryotes. *Sci Signal* 3:ra50.
44. Szurmant H, Ordal GW (2004) Diversity in chemotaxis mechanisms among the bacteria and archaea. *Microbiol Mol Biol Rev* 68:301–319.
45. Rudolph J, Tolliday N, Schmitt C, Schuster SC, Oesterhelt D (1995) Phosphorylation in halobacterial signal transduction. *EMBO J* 14:4249–4257.
46. Rudolph J, Oesterhelt D (1996) Deletion analysis of the che operon in the archaeon Halobacterium salinarium. *J Mol Biol* 258:548–554.
47. Faguy DM, Jarrell KF (1999) A twisted tale: The origin and evolution of motility and chemotaxis in prokaryotes. *Microbiology* 145:279–281.
48. Schlesner M, et al. (2012) The protein interaction network of a taxis signal transduction system in a halophilic archaeon. *BMC Microbiol* 12:272.
49. Schlesner M, et al. (2009) Identification of Archaea-specific chemotaxis proteins which interact with the flagellar apparatus. *BMC Microbiol* 9:56.
50. Allers T, Ngo HP, Mevarech M, Lloyd RG (2004) Development of additional selectable markers for the halophilic archaeon Haloferax volcanii based on the leuB and trpA genes. *Appl Environ Microbiol* 70:943–953.
51. Esquivel RN, Pohlschroder M (2014) A conserved type IV pilin signal peptide H-domain is critical for the post-translational regulation of flagella-dependent motility. *Mol Microbiol* 93:494–504.
52. Parkinson JS (1978) Complementation analysis and deletion mapping of Escherichia coli mutants defective in chemotaxis. *J Bacteriol* 135:45–53.
53. Sanders DA, Gillece-Castro BL, Stock AM, Burlingame AL, Koshland DE, Jr (1989) Identification of the site of phosphorylation of the chemotaxis response regulator protein, CheY. *J Biol Chem* 264:21770–21778.
54. Fraiberg M, et al. (2015) CheY's acetylation sites responsible for generating clockwise flagellar rotation in Escherichia coli. *Mol Microbiol* 95:231–244.
55. Ramakrishnan R, Schuster M, Bourret RB (1998) Acetylation at Lys-92 enhances signaling by the chemotaxis response regulator protein CheY. *Proc Natl Acad Sci USA* 95: 4918–4923.
56. Tripepi M, Esquivel RN, Wirth R, Pohlschröder M (2013) Haloferax volcanii cells lacking the flagellin FlgA2 are hypermotile. *Microbiology* 159:2249–2258.
57. Yan D, et al. (1999) Beryllofluoride mimics phosphorylation of NtrC and other bacterial response regulators. *Proc Natl Acad Sci USA* 96:14789–14794.
58. Jiang M, Bourret RB, Simon MI, Volz K (1997) Uncoupled phosphorylation and activation in bacterial chemotaxis. The 2.3 A structure of an aspartate to lysine mutant at position 13 of CheY. *J Biol Chem* 272:11850–11855.
59. Scharf BE, Fahrner KA, Turner L, Berg HC (1998) Control of direction of flagellar rotation in bacterial chemotaxis. *Proc Natl Acad Sci USA* 95:201–206.
60. del Rosario RCH, et al. (2007) Modelling the CheY(D10K,Yl00W) Halobacterium salinarum mutant: Sensitivity analysis allows choice of parameter to be modified in the phototaxis model. *IET Syst Biol* 1:207–221.
61. Lee S-Y, et al. (2001) Crystal structure of activated CheY. Comparison with other activated receiver domains. *J Biol Chem* 276:16425–16431.
62. Ahn D-R, Song H, Kim J, Lee S, Park S (2013) The crystal structure of an activated Thermotoga maritima CheY with N-terminal region of FliM. *Int J Biol Macromol* 54: 76–83.
63. Dyer CM, et al. (2004) Structure of the constitutively active double mutant CheYD13K Y106W alone and in complex with a FliM peptide. *J Mol Biol* 342:1325–1335.
64. Dyer CM, Vartanian AS, Zhou H, Dahlquist FW (2009) A molecular mechanism of bacterial flagellar motor switching. *J Mol Biol* 388:71–84.
65. Parkinson JS, Parker SR (1979) Interaction of the cheC and cheZ gene products is required for chemotactic behavior in Escherichia coli. *Proc Natl Acad Sci USA* 76: 2390–2394.
66. Bourret RB, Hess JF, Simon MI (1990) Conserved aspartate residues and phosphorylation in signal transduction by the chemotaxis protein CheY. *Proc Natl Acad Sci USA* 87:41–45.
67. Appleby JL, Bourret RB (1998) Proposed signal transduction role for conserved CheY residue Thr87, a member of the response regulator active-site quintet. *J Bacteriol* 180: 3563–3569.
68. Smith JG, et al. (2003) Investigation of the role of electrostatic charge in activation of the Escherichia coli response regulator CheY. *J Bacteriol* 185:6385–6391.
69. Sanna MG, Swanson RV, Bourret RB, Simon MI (1995) Mutations in the chemotactic response regulator, CheY, that confer resistance to the phosphatase activity of CheZ. *Mol Microbiol* 15:1069–1079.
70. Silversmith RE, Smith JG, Guanga GP, Les JT, Bourret RB (2001) Alteration of a non-conserved active site residue in the chemotaxis response regulator CheY affects phosphorylation and interaction with CheZ. *J Biol Chem* 276:18478–18484.
71. Schuster M, Zhao R, Bourret RB, Collins EJ (2000) Correlated switch binding and signaling in bacterial chemotaxis. *J Biol Chem* 275:19752–19758.
72. Smith JG, et al. (2004) A search for amino acid substitutions that universally activate response regulators. *Mol Microbiol* 51:887–901.
73. Barak R, Welch M, Yanovsky A, Oosawa K, Eisenbach M (1992) Acetyladenylate or its derivative acetylates the chemotaxis protein CheY in vitro and increases its activity at the flagellar switch. *Biochemistry* 31:10099–10107.
74. Liarzi O, et al. (2010) Acetylation represses the binding of CheY to its target proteins. *Mol Microbiol* 76:932–943.
75. Brendel J, et al. (2014) A complex of Cas proteins 5, 6, and 7 is required for the biogenesis and stability of clustered regularly interspaced short palindromic repeats (crispr)-derived rnas (crrnas) in Haloferax volcanii. *J Biol Chem* 289:7164–7177.
76. Tripepi M, Imam S, Pohlschröder M (2010) Haloferax volcanii flagella are required for motility but are not involved in PibD-dependent surface adhesion. *J Bacteriol* 192: 3093–3102.
77. Adler J (1966) Chemotaxis in bacteria. *Science* 153:708–716.
78. Schuhmacher JS, et al. (2015) MinD-like ATPase FlhG effects location and number of bacterial flagella during C-ring assembly. *Proc Natl Acad Sci USA* 112:3092–3097.
79. Svensson O, Malbet-Monaco S, Popov A, Nurizzo D, Bowler MW (2015) Fully automatic characterization and data collection from crystals of biological macromolecules. *Acta Crystallogr D Biol Crystallogr* 71:1757–1767.
80. Kabsch W (2010) XDS. *Acta Crystallogr D Biol Crystallogr* 66:125–132.
81. Evans PR, Murshudov GN (2013) How good are my data and what is the resolution? *Acta Crystallogr D Biol Crystallogr* 69:1204–1214.
82. McCoy AJ, et al. (2007) Phaser crystallographic software. *J Appl Crystallogr* 40: 658–674.
83. Emsley P, Cowtan K (2004) Coot: Model-building tools for molecular graphics. *Acta Crystallogr D Biol Crystallogr* 60:2126–2132.
84. Adams PD, et al. (2010) PHENIX: A comprehensive Python-based system for macromolecular structure solution. *Acta Crystallogr D Biol Crystallogr* 66:213–221.